Published OnlineFirst August 4, 2010; DOI: 10.1158/0008-5472.CAN-10-1543

Tumor and Stem Cell Biology

Cancer Research

Coactivated Platelet-Derived Growth Factor Receptor α and Epidermal Growth Factor Receptor Are Potential Therapeutic Targets in Intimal Sarcoma

Barbara Dewaele[1], Giuseppe Floris[2,4], Julio Finalet-Ferreiro[1], Christopher D. Fletcher[5], Jean-Michel Coindre[6], Louis Guillou[7], Pancras C.W. Hogendoorn[8], Agnieszka Wozniak[2], Vanessa Vanspauwen[1], Patrick Schöffski[2], Peter Marynen[1,3], Peter Vandenberghe[1], Raf Sciot[4], and Maria Debiec-Rychter[1]

Abstract

Intimal sarcoma (IS) is a rare, malignant, and aggressive tumor that shows a relentless course with a concomitant low survival rate and for which no effective treatment is available. In this study, 21 cases of large arterial blood vessel IS were analyzed by immunohistochemistry and fluorescence *in situ* hybridization and selectively by karyotyping, array comparative genomic hybridization, sequencing, phospho-kinase antibody arrays, and Western immunoblotting in search for novel diagnostic markers and potential molecular therapeutic targets. *Ex vivo* immunoassays were applied to test the sensitivity of IS primary tumor cells to the receptor tyrosine kinase (RTK) inhibitors imatinib and dasatinib. We showed that amplification of platelet-derived growth factor receptor α (*PDGFRA*) is a common finding in IS, which should be considered as a molecular hallmark of this entity. This amplification is consistently associated with PDGFRA activation. Furthermore, the tumors reveal persistent activation of the epidermal growth factor receptor (EGFR), concurrent to PDGFRA activation. Activated PDGFRA and EGFR frequently coexist with amplification and overexpression of the *MDM2* oncogene. *Ex vivo* immunoassays on primary IS cells from one case showed the potency of dasatinib to inhibit PDGFRA and downstream signaling pathways. Our findings provide a rationale for investigating therapies that target PDGFRA, EGFR, or MDM2 in IS. Given the clonal heterogeneity of this tumor type and the potential cross-talk between the PDGFRA and EGFR signaling pathways, targeting multiple RTKs and aberrant downstream effectors might be required to improve the therapeutic outcome for patients with this disease. *Cancer Res; 70(18); 7304–14. ©2010 AACR.*

Introduction

It is well established that platelet-derived growth factors (PDGF) are involved in several pathologic settings, including tumor growth (1, 2). PDGFs bind to two receptor tyrosine kinases (RTK), PDGF receptor-α (PDGFRA) and PDGF receptor-β (PDGFRB), which activate the receptor kinases and initiate a number of signaling pathways, including the RAS/extracellular signal–regulated kinase 1/2 (ERK1/2), phosphoinositide-3-kinase/AKT and protein kinase C pathways. The cellular responses to PDGF signaling involve proliferation, survival, migration, and differentiation. In mouse models, elevated PDGFRA activation leads to connective tissue hyperplasia, progressive chronic fibrosis in many organs, and sarcomagenesis (3). In humans, aberrant PDGFR signaling has been associated with a number of malignancies (4). In sarcomas, several types of genetic alterations, including gene amplification, translocations, and activating mutations, result in ligand and/or receptor overexpression (5). These aberrations may lead to dysregulated activity of PDGFRA/B. The activating mutations of *PDGFRA* in gastrointestinal stromal tumors (GIST) and the overexpression of PDGFB due to a unique *COL1A1-PDGFB* fusion in dermatofibrosarcoma protuberans serve as examples (6, 7). Imatinib mesylate, the inhibitor of the tyrosine kinase activity of BCR-ABL, which also targets PDGFRA/B, proved to be very effective for the treatment of both conditions (8, 9). There are several reports on *PDGFRA* amplifications in solid tumors, such as glioblastomas (10, 11), anaplastic oligodendrogliomas (12), and esophageal squamous cell carcinomas (13).

Authors' Affiliations: [1]Department of Human Genetics and [2]Department of General Medical Oncology, and [3]Flanders Interuniversity Institute for Biotechnology (VIB), Catholic University of Leuven; [4]Department of Pathology, University Hospitals of Leuven, Leuven, Belgium; [5]Department of Pathology, Brigham and Women's Hospital and Harvard Medical School, Boston, Massachusetts; [6]Department of Pathology, Institute Bergonié, Bordeaux, France; [7]Institute of Pathology, University of Lausanne, Lausanne, Switzerland; and [8]Department of Pathology, Leiden University Medical Center, Leiden, the Netherlands

Note: Supplementary data for this article are available at Cancer Research Online (http://cancerres.aacrjournals.org/).

R. Sciot and M. Debiec-Rychter contributed equally to this work.

Corresponding Author: Maria Debiec-Rychter, Department of Human Genetics, University of Leuven, Herestraat 49, B-3000 Leuven, Belgium. Phone: 32-16-347218; Fax: 32-16-346210; E-mail: maria.debiec-rychter@med.kuleuven.be.

doi: 10.1158/0008-5472.CAN-10-1543

Published OnlineFirst August 4, 2010; DOI: 10.1158/0008-5472.CAN-10-1543

Intimal sarcoma (IS) is a rare, lethal mesenchymal tumor arising in the large arteries, mainly the pulmonary artery and the aorta. Presumably, these sarcomas develop from the subendothelial cells of the blood vessel wall located in the intima (14). The defining feature is the predominant intraluminal growth with obstruction of the lumen of the vessel of origin and embolic tumor dissemination (15). On histology, IS usually displays features of a poorly differentiated sarcoma, composed of spindle cells, with varying degrees of atypia, mitotic activity, nuclear polymorphisms, and necrosis (16). Some tumors may show considerable heterogeneity in terms of extracellular matrix and tumor cell composition. Large myxoid regions or an epithelioid component can be observed, as well as areas of rhabdomyo-, angio-, or osteosarcomatous differentiation (17–21). Angiosarcoma and leiomyosarcoma are the most important entities that have to be included in the differential diagnosis. The clinical presentation of IS is often not specific and related to tumor emboli (15). Pulmonary IS behaves very aggressively on site, conferring lung infiltrations in 40% of the patients (22, 23). Aortic IS mostly arises in the abdominal aorta. Arterial embolic tumor dissemination might result in distant metastases involving the bone, peritoneum, liver, and mesenteric lymph nodes (15). The prognosis of IS is poor, with a mean survival time of about 12 months (24).

To date, the understanding of the histogenesis and molecular mechanisms leading to the development of IS remains fragmentary. In recent years, recurrent molecular genetic events associated with IS development have been reported based on the analysis of a few cases. By comparative genomic hybridization (CGH), recurrent amplification of the regions 4q12 and 12q13-q15 was described in a subset of IS (25). Amplification of the chromosomal region 12q13-q15 was reported in 75% of these tumors (14, 25). Multiple genes in this region, such as *MDM2, SAS, CDK4*, and *GLI1*, are frequently amplified in many types of human cancer (14, 26). Notably, amplification of the *PDGFRA* gene, which maps to chromosome 4q12, was reported in 5 of 8 (62.5%) pulmonary artery IS (25). In a more recent report, deregulated copy numbers of *PDGFRA/PDGFRB, KIT*, and *EGFR* were described in seven examined IS cases, and the activation of the PDGFRs and EGFR has been disclosed by biochemical assays in one of these IS cases (24).

Due to the rareness of IS, these lesions have been a neglected area and there is a lack of specific biomarkers. The therapy is currently limited to surgery (23). In this study, we aimed to identify potential novel diagnostic markers and molecular targets for the treatment of IS. To this aim, we have performed an integrated histopathologic, cytogenetic, molecular, and biochemical analysis of a large cohort of 21 cases with IS. In view of the clinical availability of several therapeutic agents against RTKs, we have focused on the relevance of activation of RTKs in the pathobiology of IS and on the inhibitory effect of RTK inhibitors on primary IS cells.

Materials and Methods

Patients and histopathology

The present study included 21 patients (11 females and 10 males; age range, 27–74 years; median age, 52 years; Table 1). The tumors were located in the pulmonary artery trunk (n = 12), right or left pulmonary artery (n = 3), heart (n = 4), femoral artery (n = 1), and splenic artery (n = 1), and one presented as a femoral embolus from the aorta primary site.

Histopathologic examination was performed on formalin-fixed, paraffin-embedded tissues. Five-micrometer sections were used for routine H&E and immunohistochemical stainings (avidin-biotin-peroxidase complex method), using the following monoclonal (mc) and polyclonal (pc) antibodies: α-smooth muscle actin (α-SMA; mc, 1/100; DAKO), desmin (mc, 1/20; ICN), CD31 (mc, 1/50; DAKO), CD34 (mc, 1/10; Becton Dickinson), MDM2 (mc, 1/100; Invitrogen, Life Technologies), CD117 (pc, 1/250; DAKO), EGFR (EGFR PharmDx Kit, DAKO), and human epidermal growth factor receptor 2 (HER2; HercepTest, DAKO). EGFR and HER2 protein expression was reported as membranous brown staining of neoplastic cells using a three-tier system ranging from 1+ (weak intensity) to 3+ (strong intensity).

Cytogenetic analysis

Karyotyping was performed on primary tumor cells from three cases after 7 days in culture.

Array-CGH analysis

Genomic DNA was isolated from eight frozen tumor tissues using the High Pure PCR Template Preparation Kit (Roche Diagnostics). The Agilent Human Genome Microarray Kit 244A (Agilent Technologies) was used to perform array-CGH (aCGH) analysis. Labeling, hybridization, washing, and scanning were carried out in accordance with the protocols provided by the manufacturer. The Agilent Feature Extraction software (version 10.5.1.1) was used to process the images obtained from the scanner (Agilent DNA microarray scanner, with up to 2-μm precision) and to generate a text file (FE file). Subsequently, the FE files were analyzed using the Agilent Genomic Workbench Standard Edition 5.0.14 software based on the HG18 genome build. The ADM-2 algorithm was chosen for reporting copy number aberrations (CNA). Regions with a log 2 ratio >2 were considered as amplified, and regions with a log 2 ratio <−1 were considered as homozygously deleted. The data were submitted to the Gene Expression Omnibus database (accession no. 15834535).

Fluorescence *in situ* hybridization

Fluorescence *in situ* hybridization (FISH) analysis was performed on all 21 cases as previously described (27). Pretreatment and enzyme digestion were done using the SPoT-Light Tissue Pretreatment Kit (Invitrogen). Chromosome 4 and *PDGFRA* copy numbers were determined by cohybridization of Spectrum Green (SG)–labeled centromer-specific probe CEP4 (Vysis, Inc., Abbott Laboratories) and Spectrum Orange (SO)–labeled bacterial artificial chromosome (BAC) DNA probe RP11-231C18, which maps to *PDGFRA* (Research Genetics). For evaluation of the integrity of *PDGFRA*, BAC probes centromeric (RP11-3H20-SO) and telomeric (RP11-24O10-SG) to the *PDGFRA* locus (both from Research Genetics) were used. The coamplification of *PDGFRA* and *MDM2* or *EGFR* on a cellular level was determined by cohybridization of

Published OnlineFirst August 4, 2010; DOI: 10.1158/0008-5472.CAN-10-1543

Table 1. Clinical features, immunohistopathologic data, and FISH results of 21 IS cases

No.	Sex	Age (y)	Site	Immunostaining								FISH (%)			
				α-SMA	Desm.	CD31	CD34	MDM2	CD117	EGFR	HER2	PDGFRA	MDM2	EGFR	HER2
1	F	42	r.p.a.	++	+–	++	+–	+–	–	3+d/C+M	–	67 a.	74 a.	60 t.	neg.
2	M	70	p.a.	+–	n.d.	–	–	++f	–++f/weak	2+d/C+M	1+	18 a.	80 a.	35 p.	neg.
3	F	27	p.a.	+–	n.d.	–	–	n.d.	–	3+d/C+M	–	85 a.	neg.	29 p.	n.d.
4	F	62	heart	–	–	–	–	+++	–	1+f/C+M	n.d.	70 a.	54 a.	35 p.	n.d.
5	F	28	heart	–	–	–	n.d.	n.d.	–	2+d/M	1+	90 a.	30 a.	46 p.	n.d.
6	M	45	p.a.	–	–	–	–	++f	–	1+f/C+M	n.d.	65 a.	21 a.	70 p.	n.d.
7	F	62	r.p.a.	++	–	–	–	++	–	3+d/C+M	1+	12 a.	83 a.	34 p.	n.d.
8	F	62	f.a.	++	n.d.	–	n.d.	–	–	1+f/C+M	–	neg.	neg.	90 t.	neg.
9	F	49	p.a.	+–	++	–	–	++	n.d.	2+d/C+M	–	31 a.	62 a.	12 p.	neg.
10	M	50	p.a.	–	–	–	n.d.	+–	n.d.	1+f/C	–	53 a.	15 a.	35 p.	neg.
11	M	74	p.a.	n.d.	n.d.	n.d.	n.d.	n.d.	n.d.	3+d/M	n.d.	43 a.	n.d.	52 p.	n.d.
12	M	52	p.a.	n.d.	n.d.	n.d.	n.d.	n.d.	n.d.	3+d/C+M	–	47 p.	n.d.	31 a.	n.d.
13	M	60	p.a.	n.d.	n.d.	n.d.	n.d.	–	–+	1+f/C+M	–	26 a.	neg.	neg.	neg.
14	F	36	p.a.	++	n.d.	n.d.	n.d.	–	–++f/weak	1+f/M	–	17 p.	neg.	neg.	15 p.
15	M	71	p.a.	n.d.	n.d.	n.d.	n.d.	n.d.	n.d.	2+f/C+M	–	40 a.	n.d.	neg.	neg.
16	M	74	f.e.	–	–	++	+–	++	–	–	–	51 a.	85 a.	neg.	neg.
17	F	68	p.a.	n.d.	n.d.	n.d.	n.d.	n.d.	n.d.	2+f/C+M	–	44 a.	n.d.	46 p.	neg.
18	F	30	l.p.a.	–	n.d.	n.d.	n.d.	–	–+f/weak	1+f/C+M	–	21 a.	neg.	neg.	neg.
19	M	31	heart	+–	–	–	+–	++	–	2+d/M	n.d.	80 a.	75 a	35 a.	n.d.
20	F	33	p.a.	+–	–	–	nd	+++	–	3+d/C+M	n.d.	79 a.	82 a	52 p.	n.d.
21	M	62	a.l.	–	–	–	+–	+++	–	n.d.	n.d.	84 p.	80 p	75 p.	n.d.

Abbreviations: Desm., desmin; F, female; M, male; r., right; l., left; p.a., pulmonary artery; f.a., femoral artery; f.e., femoral artery embolism; a.l., arteria lienalis; d, diffuse staining; f, focal staining; C, cytoplasmic staining; M, membranous staining; a., amplification; p., polysomy; t., trisomy; n.d., not done; neg., no copy number changes.

PDGFRA/RP11-24O10-SO and *MDM2*/RP11-1064P9-SG or *PDGFRA*/RP11-24O10-SG and *EGFR*/RP11-231C18-SO labeled probes. The BAC DNA was isolated and labeled with fluorochrome dyes using standard techniques. Detection was performed as previously described (27). In addition, the *MDM2, EGFR*, and *HER2* gene copy numbers were investigated using the double-color locus-specific identifier (LSI) MDM2-SO/CEP12-SG (Applied Biosystems/Ambion, Life Technologies), LSI EGFR-SO/CEP7-SG (Vysis), and LSI HER2-SO/CEP17-SG (Vysis) probes, respectively, according to the manufacturers' recommendations. Slides were counterstained with 0.1 μmol/L 4,6-diaminido-2-phenylindole in an antifade solution and viewed under a fluorescence microscope equipped with an ISIS digital image analysis system (MetaSystems). Signal copy numbers were counted from 100 nonoverlapping nuclei from at least three different areas and the percentage of affected nuclei was recorded. Chromosome polysomy was defined as >4 gene signals per nucleus paralleled by similar increases in chromosome centromere signals in at least 10% of tumor cells. A gene/CEP ratio of >2 in at least 10% of tumor cells was defined as specific gene amplification.

Mutation analysis

Mutational analysis was performed on genomic DNA extracted from frozen tumor tissues (n = 6). The whole coding sequence of the *PDGFRA* gene and the sequences coding for the juxtamembrane and/or kinase domains of *PDGFRB* and *EGFR* were amplified. Specific primers for amplified fragments are listed in Supplementary Table S1. The PCR products were purified and bidirectionally sequenced using the ABI PRISM 3130 XL Genetic Analyzer (Applied Biosystems).

RTK activation profiling

The expression and activation of RTKs and their downstream signaling pathways were analyzed using the Proteome Profiler Array kits (R&D Systems) according to the manufacturer's protocol and using 500 μg of protein lysate per array. The images were captured and the level of RTK activation was densitometrically quantified with AIDA software (TBC Software, Inc.). The intensity values of the probes and the local background of the probes were log 2 transformed to obtain a more symmetrical distribution, and the difference between these two resulted in a log 2 transformed ratio (further referred to as log 2 intensity ratios). Subsequently, the mean of the log 2 intensity ratios for each kinase within an array was calculated. Probes with a log 2 intensity ratio higher than the mean plus SD were considered as significantly activated.

Western immunoblotting

Tumor specimens (n = 7) were snap-frozen at –80°C and used for Western immunoblotting. A primary GIST that harbored a *PDGFRA*-D842V mutation and the human

Published OnlineFirst August 4, 2010; DOI: 10.1158/0008-5472.CAN-10-1543

GIST882 (28) and SQD9 squamous cell carcinoma cell lines (29) were incorporated as controls. Cell lysis, SDS-PAGE, and immunoblotting were carried out as previously described (30). Membranes were immunoblotted sequentially using rabbit antibodies against phospho-EGFR (Tyr845; R&D Systems), total EGFR (Santa Cruz Biotechnology), phospho-PDGFRA (Tyr754; Santa Cruz Biotechnology), total PDGFRA (Santa Cruz Biotechnology), phospho-ERK1/2 (Cell Signaling), total ERK1/2 (Invitrogen, Life Technologies), phospho-AKT (Cell Signaling), total AKT (Cell Signaling), and total actin (Sigma-Aldrich), diluted in 5% blocking reagent. The horseradish peroxidase–conjugated antirabbit IgGs were used for enhanced chemiluminescence visualization (Thermo Scientific).

Ex vivo assay

Primary cells from a collagenase-disaggregated tumor specimen from case no. 1 were used for the cell cultures, as previously described (31). In short, cells were grown for 3 days in DMEM supplemented with 10% fetal bovine serum, MITO$^+$ serum extender (used according to the manufacturer's recommendation; BD Biosciences), 30 μg/mL bovine pituitary extract (BD Biosciences), 0.1 mmol/L nonessential amino acids, and 1.0 mmol/L sodium pyruvate. Cells were exposed to imatinib, dasatinib, or vehicle alone for 2 hours at 37°C. After a wash in ice-cold PBS, cells were lysed and used for Western immunoblotting as described above.

Compounds

The inhibitors imatinib (Glivec/Gleevec, Novartis) and dasatinib (BMS-354825, Bristol-Myers Squibb) were provided by MedImmune, Inc. The inhibitors were diluted in culture medium directly before use.

Results

Histopathology

On histology, the tumors showed a variable morphology, ranging from spindle cell proliferations with variable cellularity to islands of high anaplastic pleomorphic tumor cells with atypical mitotic figures (Supplementary Fig. S1). Low-grade– and high-grade–appearing areas were simultaneously present in all tumors. The matrix was usually collagenous, but on occasion was very myxoid; in one case, osteoid production was observed. Immunohistochemistry revealed focal and weak expression of CD31, CD34, and desmin in 10% to 20% of cases (Table 1). About half of the tumors investigated were α-SMA positive. EGFR was expressed in all but one case, although the staining pattern was heterogeneous, from strongly diffuse (3+; $n = 6$) to intermediate (2+; $n = 7$) or low and focal (1+; $n = 7$). MDM2 staining was positive in 52% of examined cases. CD117 (KIT) expression was rare and occurred in only two tumors mainly as focal and weak staining.

Karyotype analysis

All three IS tumors featured a polyploid range of chromosome number and complex structural rearrangements, with the presence of homogeneously staining regions within unidentified markers in two cases (nos. 1 and 4) and double minutes in the third case (no. 19; data not shown).

aCGH study

Using high-resolution oligonucleotide aCGH, we studied CNAs in eight cases for which frozen tissue was available. There was a median of 64 gains (range, 36–83) and 42 losses (range, 13–63) per tumor. CNAs affecting six or more tumors (≥75% of cases) were identified on chromosomes 3q, 4q, 7p, 8q, 9p, 10q, and 12q (Table 2; Fig. 1). Major segments of high-level amplification were localized within chromosomes 1, 3, 4, 6, 8, 9, 12, 16, 21, 22, and X (Supplementary Table S2). Six of eight tumors showed chromosome 4q12 amplification, with the common region (54.78–55.21 Mb) containing only the *PDGFRA* gene (Fig. 2). The region at 12q15 (68.32–68.45 Mb) was amplified in 50% of the cases; the common region of amplification encompassed the *BEST3* gene (the encoded protein is a Ca-activated Cl channel candidate in the development of vascular smooth muscle cells; ref. 32). Three chromosomal regions were amplified in 37.5% of cases, that is, the chromosomal regions 12q14.1 (*KUB3*), 12q15 (67.43–67.79 Mb; containing *MDM2, SLC35E3*, and *CPM* genes), and 22q11.23 (*GSTT1*). Four additional regions, 8p11.23-p11.22, 12q13.3-q14, 12q14.2-q14.3, and Xp21.1, were amplified in two cases each. Seventeen other amplified regions, which harbor known cancer-related genes, were observed in single cases.

Homozygous deletions were found on chromosomes 3, 5, 6, 7, 9, 10, 12, 13, 18, 20, and 22 (Supplementary Table S2). The homozygous deletions at 9p21.3-p21.2 (21.89–25.65 Mb), covering the *CDKN2A/CDKN2B* loci, were found in three of eight tumors. In addition, loss of one copy of *CDKN2A/CDKN2B* loci was revealed in three additional cases. This finding indicates that loss of *CDKN2A/CDKN2B*, although not tumor type specific, may be important for IS development and/or progression. The three chromosomal sub-bands—3p26.2 (*ITPR1*), 3p14.1 (*FOXP1*), and 18q22.3 (*FBXO15*)—were homozygously lost in two cases each. Twelve other homozygous deletions were found in one case each, and some of these deletions harbor known putative tumor suppressor genes.

FISH analysis

The eight tumors analyzed with 244A Agilent array and 13 additional paraffin-embedded IS were evaluated by FISH (Table 1; Fig. 3) using specific probes for *PDGFRA, EGFR, MDM2*, and *HER2*. The *PDGFRA* amplification was the most prevalent change, found in 17 of 21 (81%) cases (Fig. 3A). Notably, two tumors (nos. 2 and 7) that showed focal *PDGFRA* amplification (from 12% to 18% affected cells) by FISH did not reveal this amplification by the parallel aCGH analysis (Figs. 2 and 3B). This finding indicates that the FISH technique is more suitable than aCGH for detecting the focal CNA in the context of cytogenetically heterogeneous and polyploid tumors. Three other IS showed high-level polysomy of *PDGFRA*, and only one case did not reveal any CNA of *PDGFRA*. Importantly, none of the examined cases showed a rearrangement of *PDGFRA*.

Published OnlineFirst August 4, 2010; DOI: 10.1158/0008-5472.CAN-10-1543

Table 2. Recurrent copy number losses and gains in IS by aCGH

	Regions lost or gained in ≥6 cases			
Cytogenetic location	**Start-end (Mb)***	**Size (Mb)**	**Frequency**	**Examples of candidate genes**
Copy number losses				
3q12.1	99.98-100.07	0.09	0.75	*DCBLD2*
3q12.1-q12.2	100.50-101.66	1.16	0.75	*FILIP1L*
3q12.3-q13.31	103.31-118.66	15.35	0.75	
3q13.33-q21.2	121.12-126.21	5.09	0.75	*MUC13, PTPLB, DIRC2, EAF2, RABL3*
3q21.2-q21.3	126.67-130.74	4.07	0.75	*RAB34*
9p21.3-p21.2	21.69-27.13	5.43	0.75	*CDKN2A, CDKN2B*
10q22.1	74.24-74.38	0.13	0.75	*PLA2G12B*
12q12	93.95-94.38	0.42	0.75	
12q23.1	95.36-95.85	0.49	0.75	*NEDD1*
12q23.1	97.52-98.27	0.75	0.75	*IKIP, APAF1*
Copy number gains				
4q12	54.42-54.94	0.52	0.88	*PDGFRA, CHIC2, GSX2*
7p22.3-p14.2	1.09-35.67	34.58	0.75	*PLEKHA8, SKAP2, IGF2BP3, IL6, RAPGEF5*
8q11.21-q23.1	48.21-110.23	62.02	0.75	*LRP12, BAALC, CCNE2, GEM, PLAG1, MOS, LYN, CEBPD, PREX2*
12p11.22-p11.21	29.94-31.04	1.09	0.75	*CAPRIN2, TSPAN11*
12q13.3	55.57-55.77	0.20	0.75	*NAB1*
12q13.3-q14.1	55.81-56.74	0.93	0.75	*GLI1, TSPAN31, CDK4, AGAP2, DDIT3*
12q14.1	59.27-60.20	0.93	0.75	
12q14.2-q14.3	62.90-65.53	2.63	0.75	*IRAK3, HMGA2, TBK1*
12q14.3-q15	65.94-68.44	2.51	0.75	*FRS2, YEATS4, MDM2, SLC35E3, RAP1B, MDM1, DYRK2*
12q15	68.55-68.62	0.08	0.75	*C12orf28*

*Minimal region gained or lost.

The *MDM2* gene was amplified in a large subset of tumors in our series (11 of 17 cases; 65%) and one case showed *MDM2* gene polysomy.

In total, 16 (76%) tumors showed either *EGFR* amplification (n = 2) or *EGFR* aneuploidy (n = 14). Additionally, the status of the gene encoding HER2, a close family member and an important dimerization partner of EGFR, was investigated. There was polysomy of *HER2* in one case. By immunohistochemistry, strong EGFR-positive staining tended to correlate with *EGFR* gene amplification and aneuploidy, suggesting that the amplified *EGFR* is transcribed and translated to protein.

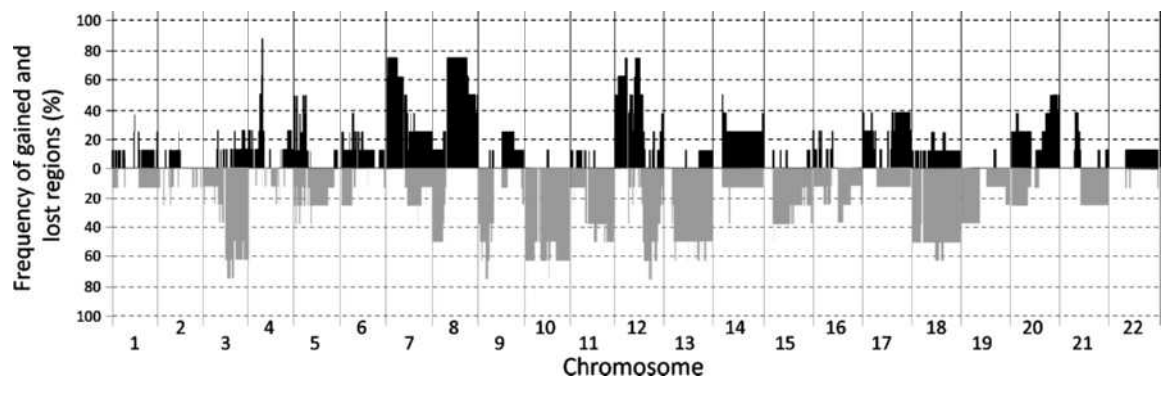

Figure 1. Frequency of CNA detected by 244A Agilent aCGH in eight IS. The genomic positions of the most frequent imbalances are presented in Table 2.

Published OnlineFirst August 4, 2010; DOI: 10.1158/0008-5472.CAN-10-1543

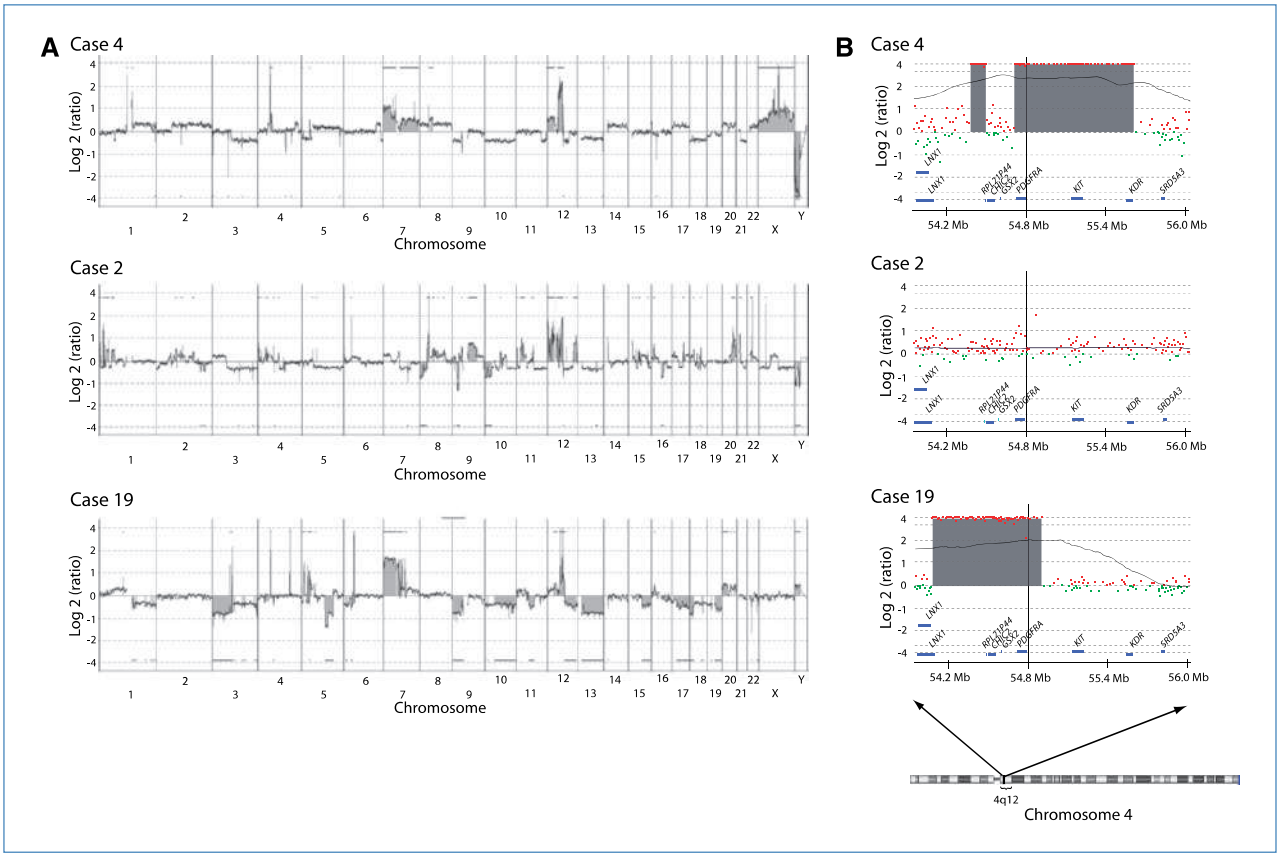

Figure 2. A, representative CNA profile by 244A Agilent aCGH: case 4, case 2, and case 19. The individual array probes are arranged according to their genomic location (*X* axis) and their respective tumor/reference log 2 ratios (*Y* axis). B, aCGH profiles by 244A Agilent of a selected region of chromosome 4q12 (54.2–56.0 Mb). Case 4 and case 19 show a high level of amplification of this region, with the smallest common region of amplification containing only the *PDGFRA* gene. The low level and focal amplification of *PDGFRA* in case 2, as identified by FISH (Fig. 3B), is not detected by aCGH.

In the subsequent step of FISH analysis, we have explored the colocalization of *PDGFRA, EGFR*, and *MDM2* amplicons on a cellular level in three cases (nos. 1, 4, and 19). Coamplification of *PDGFRA* with *MDM2* or *EGFR* was observed as partially overlapping large-clustered amplicons and/or as multiple, scattered signals (Fig. 3C and D). Interestingly, subpopulations of tumor cells with mutual or exclusive amplification of *PDGFRA* and *MDM2* or *EGFR* coexisted in each of the examined specimens.

Mutation analysis

No activating mutations were identified in *PDGFRA/B* and *EGFR* in the six IS cases (nos. 1, 2, 3, 7, 9, and 10) analyzed.

RTK phosphorylation profiling using phospho-RTK and phospho-kinase antibody arrays

All seven analyzed tumors revealed strongly coactivated PDGFRA and EGFR kinases (Fig. 4). Six cases concurrently showed phosphorylation of PDGFRB. Four cases concomitantly showed low-level phosphorylation of EPHB2, and three cases also had low-level phosphorylation of AXL. Strikingly, there was no detectable activation of KIT or vascular endothelial growth factor receptors, nor activation of the members of the SRC-family proteins. By analyzing the signaling pathways (the profiles of 46 kinases and protein substrates), CREB, eNOS, TP53, JUN, STAT5B, and AMPKα1 were found to be the most frequently and strongest phosphorylated proteins (Supplementary Table S3; Fig. 4).

The consistent protein expression and activation of PDGFRA and EGFR were confirmed by Western immunoblotting or immunohistochemistry (Supplementary Fig. S2; Table 1). By immunoblotting, both the AKT and ERK1/2 downstream signaling pathways were activated, the latter to a much stronger level, which is in line with PDGFR/EGFR–driven tumors (31, 33, 34).

Ex vivo biochemical assay using primary IS cells

We examined the consequences of PDGFRA inhibition with imatinib and dasatinib in primary IS cultures from case no. 1. Both inhibitors caused a dose-responsive decrease in PDGFRA phosphorylation (Fig. 5). Dasatinib completely blocked the phosphorylation of the target PDGFRA at 0.1 μmol/L. In contrast, 0.5 μmol/L imatinib only slightly affected PDGFRA activation, and 5.0 μmol/L imatinib was needed to completely abrogate PDGFRA phosphorylation. Hence, dasatinib inhibited PDGFRA at much lower (clinically

Published OnlineFirst August 4, 2010; DOI: 10.1158/0008-5472.CAN-10-1543

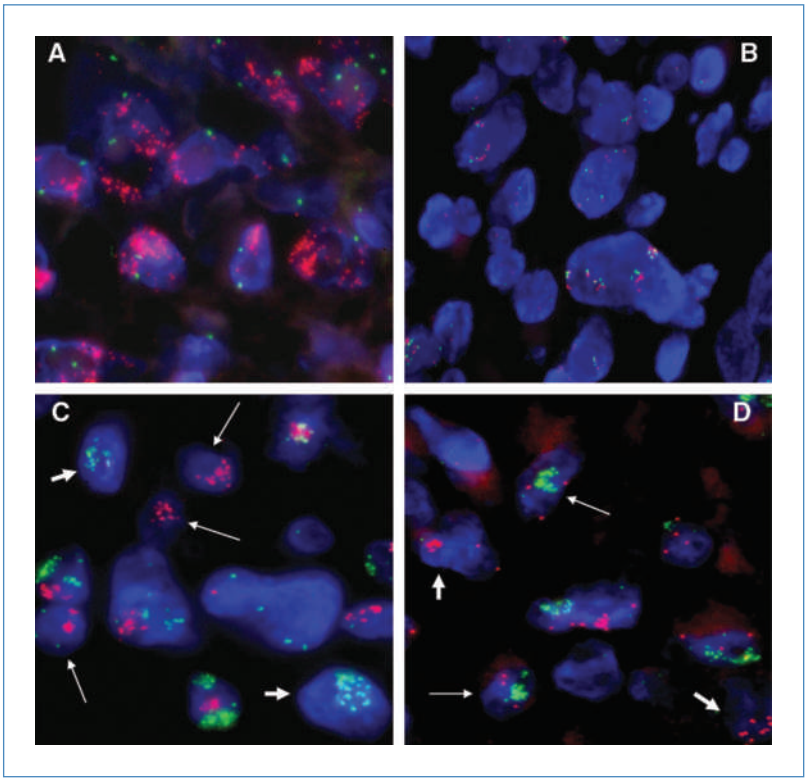

Figure 3. Representative examples of dual-color interphase FISH images of paraffin sections of IS. A, case 5, showing high-level amplification of *PDGFRA* (>90% of nuclei) as detected by the cohybridization of SO-labeled BAC *PDGFRA*/RP11-24O10 DNA probe (red signals) and SG-labeled chromosome 4 CEP (green signals). B, using the same combination of probes, case 2 reveals low-level and focal (12% of cells) amplification of *PDGFRA*. Of note, this amplification is not detected by aCGH, as pictured in Fig. 2B. C, the cohybridization of *PDGFRA*/RP11-24O10-SO (red signals) and *MDM2*/RP11-1064P9-SG (green signals) labeled probes in case 19 reveals cells with exclusive amplification of *PDGFRA* (long arrows) or *MDM2* (short arrows), intermingled with cells showing separate amplicons for both genes. D, the same intratumor heterogeneity is detected by the cohybridizations of *PDGFRA*/RP11-24O10-SG (green signals) and *EGFR*/RP11-231C18-SO (red signals) labeled probes; cells with exclusive amplification of *PDGFRA* and *EGFR* are indicated by long and short arrows, respectively.

achievable) concentrations. Using p-AKT and p-ERK1/2 proteins as molecular surrogates of downstream RTK signaling, we found that both the AKT and ERK1/2 pathways were activated in untreated IS primary cells. Importantly, although PDGFRA activation was completely abolished with 5 μmol/L imatinib, the downstream signaling pathways were still active. In contrast, complete inactivation of PDGFRA was associated with substantial inactivation of both ERK1/2 and AKT with 0.5 μmol/L dasatinib. This suggests that other dasatinib targets, next to PDGFRA, might be responsible for the inactivation of downstream ERK1/2 signaling by dasatinib.

Discussion

Using a variety of methodologic approaches, we aimed for a comprehensive characterization of IS in search for relevant diagnostic biomarkers and therapeutic targets.

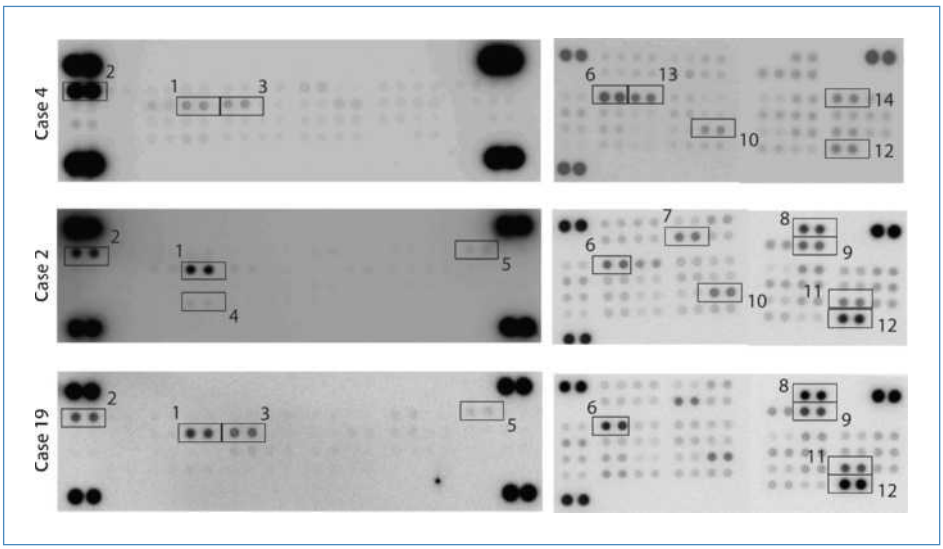

Figure 4. The PDGFRA and EGFR kinases and their downstream signaling intermediates are activated simultaneously in IS. Representative images from phospho-RTK (left) and phospho-kinase (right) arrays from whole-tumor lysates of case 4, case 2, and case 19. Each kinase is spotted in duplicate. The pairs of dots in each corner are positive controls. Each pair of the most positive kinase dots is denoted by a numeral, with the identity of the corresponding kinases listed as follows: 1, PDGFRA; 2, EGFR; 3, PDGFRB; 4, EPHB2; 5, AXL; 6, CREB(S133); 7, AMPKα1(T174); 8, TP53(S392); 9, TP53(S46); 10, STAT5b(Y699); 11, JUN(S63); 12, eNOS(S1177); 13, HSP27 (S78/S82); 14, P27 (T198).

Published OnlineFirst August 4, 2010; DOI: 10.1158/0008-5472.CAN-10-1543

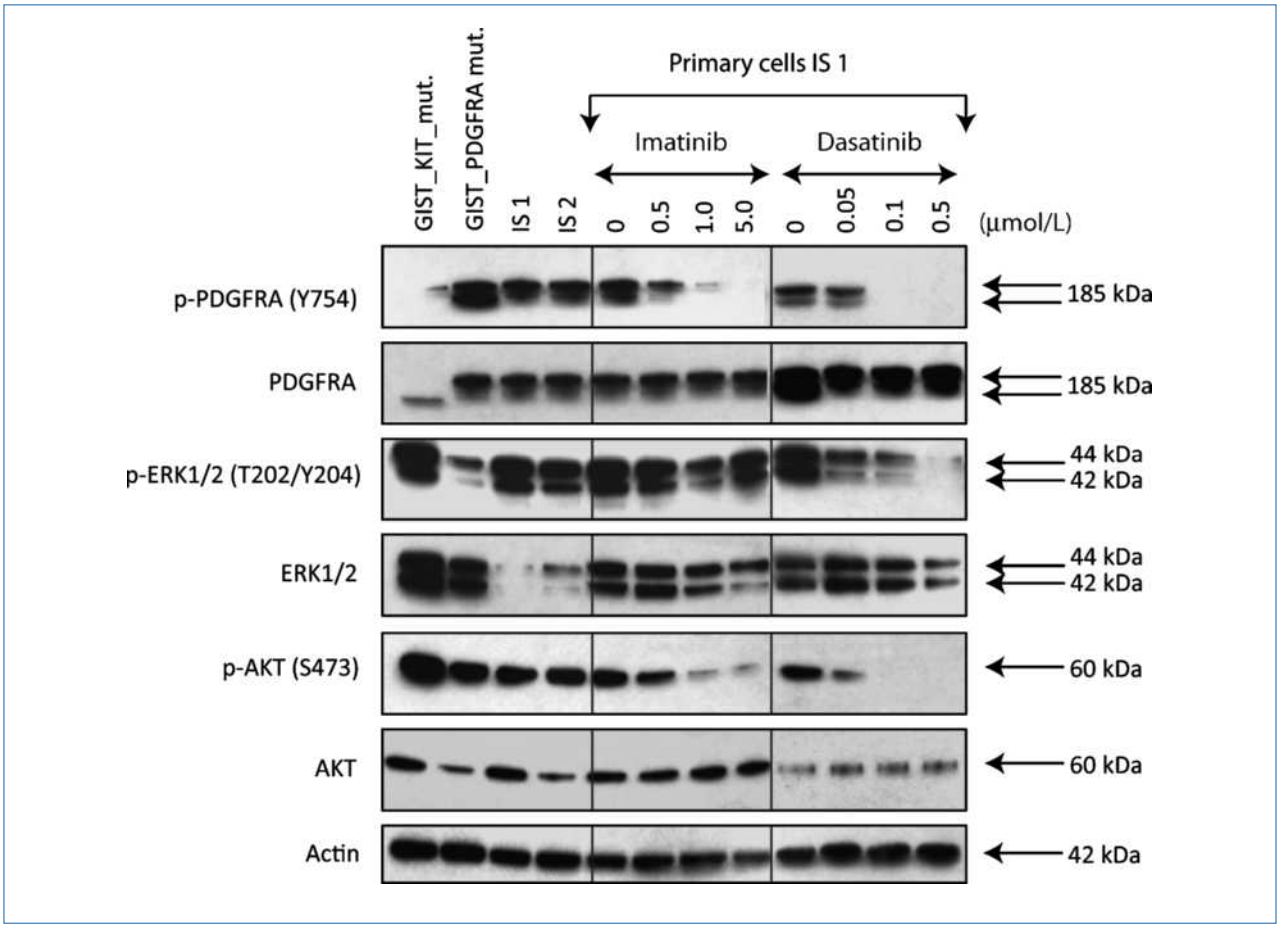

Figure 5. Immunoblots showing the effect of the 2-h exposure of the primary IS cells to increasing doses of imatinib or dasatinib on the phosphorylation of PDGFRA and the downstream effectors ERK1/2 and AKT. Actin served as a loading control. The lysates from the frozen tissue specimens, IS 1 (case 1) and IS 2 (case 2), and from the GISTs carrying KIT^{K642E} (GIST_KIT mut.) or $PDGFRA^{D561V}$ (GIST_PDGFRA mut.) mutations were run in parallel as control samples.

As expected, high-resolution 244A Agilent aCGH revealed complex CNA in all examined cases across the genome, including previously recognized oncogenes and tumor suppressor genes, as well as completely novel loci. Most importantly, high-level amplifications or copy number gains frequently involved chromosomal regions that contain the *PDGFRA, EGFR*, and/or *MDM2* genes.

Accordingly, *PDGFRA* amplification and high-level polysomy by FISH were present in 81% and 15% of tumors, respectively. Remarkably, using high-resolution array, we were able to delineate the common region of 4q12 amplification to 54.78 to 55.21 Mb, containing only the *PDGFRA* locus. Thus, *PDGFRA* is the most likely target for amplification in IS. Our findings are comparable to the results reported previously on smaller IS cohorts (24, 25). To the best of our knowledge, no other sarcoma reported thus far presents consistent *PDGFRA* amplification (35). Thus, given its specificity and high frequency of occurrence, the *PDGFRA* amplification in IS might be considered as a molecular hallmark of the entity. Importantly, *PDGFRA* amplification, detected by FISH, is a valuable marker for IS diagnosis, distinguishing IS from the other undifferentiated sarcomas known to reside in similar anatomic sites.

The amplification of the 12q15 region, harboring the *MDM2* locus, was another consistent and frequent feature revealed by aCGH. Amplification and consequent upregulation of the *MDM2* oncogene represent a recurrent molecular feature of many sarcomas, such as de-differentiated liposarcomas (36), and it was also reported in IS (14, 24, 25). The extended FISH analysis revealed that 65% of tumors have *MDM2* amplification in our cohort. *MDM2* amplification was closely correlated with the protein expression of this oncogene, as evidenced by immunohistochemistry. Because the amplification or overexpression of MDM2 has been found in many cancers, inhibiting MDM2 and thereby reactivating TP53 in cancer cells is an emerging new therapeutic strategy. Nutlin-3 and MI-219 are MDM2 inhibitors with desirable pharmacologic properties and are in advanced preclinical development or early-phase clinical trials (37). Interestingly, cancer cell

Published OnlineFirst August 4, 2010; DOI: 10.1158/0008-5472.CAN-10-1543

lines with *MDM2* gene amplification were shown to be more sensitive to Nutlin-3 than cell lines lacking this amplification (38).

The gain of chromosome 7p, encompassing the *EGFR* locus, was accounted for in six of eight cases analyzed by aCGH in the present study. High-level *EGFR* aneuploidy (or rarely amplification) was confirmed by FISH (76% of cases). EGFR belongs to the ERBB family of RTKs, which recognize at least 11 known ligands (39, 40). There is ample evidence of amplified and activated forms of EGFR in many human cancers, and drugs that specifically target EGFR show promise in inhibiting the growth of certain tumor types (39). Sato and colleagues showed that 168 of 281 (60%) adult soft tissue sarcomas overexpressed EGFR (41); this overexpression significantly correlated with higher histologic grade, poorer survival, and chemoresistance. It is noteworthy that gefitinib, an EGFR inhibitor, has shown potential antitumor effects in several sarcoma cell lines when used in combination with irinotecan (42).

To define the compendium of coactivated RTKs in IS, we used an antibody array that allows simultaneous assessment of the phosphorylation status of 42 RTKs. Of utmost importance and coherent with the crucial biological role for the IS pathogenesis, the PDGFRA and EGFR kinases were consistently activated in all seven investigated cases of our study. The PDGFRB kinase was activated in a smaller subgroup of tumors. The coactivation of multiple RTKs is not a distinctive feature of IS because similar patterns were reported in other tumor types (43–46). Importantly, the concomitant activation of multiple RTKs serves to reduce dependence on a single RTK for the maintenance of critical downstream signaling and, thus, renders such tumors refractory to single-agent RTK inhibition.

The recurrent high-level amplification and strong activation of PDGFRA in absence of resistance mutations prompted us to investigate the effect of the PDGFRA inhibitors imatinib and dasatinib in IS. Both inhibitors were able to specifically inhibit PDGFRA kinase activity, but dasatinib showed higher potency. The stronger inhibitory capacities of dasatinib toward PDGFR in reference to imatinib were previously shown in rat A10 vascular smooth muscle cells (47). Additionally, dasatinib showed a more effective inhibition of downstream ERK1/2 and AKT signaling than did imatinib in primary IS tumor cells. It is likely that IS cells under PDGFR-targeted treatment are still able to maintain downstream signaling through the ERK1/2 and AKT pathways due to EGFR coactivation. By RTK array, the propagated *ex vivo* tumor cells lacked activation of SRC family members. Thus, the possibility that inhibition of SRC-family kinases could contribute significantly to the inhibitory effect of dasatinib on the PDGFR downstream signaling pathway is remote. Yet, the discrete SRC activation to levels not discernible by our technique could still exist in the tested cells, rendering them more prone to dasatinib inhibition. Interestingly, it was recently shown in lung cancer that dasatinib may reduce EGFR activation through the inhibition of SRC, which mediates the phosphorylation of the Y845 residue in the receptor (48–50).

It is essential to emphasize that the success of the therapy in IS might strongly depend on the genetic context of the tumor, which is complex, as indicated by the numerous CNAs of cancer-related genes identified by aCGH. The *CDKN2A/CDKN2B* losses were recurrent in IS in our cohort. This is in line with previous studies that have shown a synergistic effect on neoplasia induction when aberrant oncogenic PDGFRA signaling is combined with loss of the tumor suppressors *CDKN2A/CDKN2B* (3, 47). Moreover, the TP53 pathway seems to be frequently affected in IS (e.g., common *MDM2/CDK4* amplifications), pointing to confounding factors that might attenuate the response to RTK inhibition.

Second, an important and hitherto unreported finding in our study is the concomitant existence of cells with exclusive amplification and cells with coamplification of *PDGFRA, EGFR*, or *MDM2* within a single tumor, as detected by FISH. The mechanism leading to gene coamplification remains to be clarified. In breast cancer, the coamplification most likely arises by the selection of clones that have both foci amplified rather than as a direct result of prior fusions (51). In our study, the populations with coamplification and single amplifications seem to be able to coexist independently. It is equally important to keep in mind that selection of certain populations might happen once targeted treatment is started. This provides a rationale for multitargeted treatment of IS.

In conclusion, *PDGFRA* amplifications are common and consistently associated with the activation of this gene in IS. Activation of EGFR is concurrent to PDGFRA activation and may coexist with amplification and overexpression of MDM2. Our data provide a rationale for the targeted treatment of IS with specific PDGFRA, EGFR, and MDM2 inhibitors. Dasatinib may be more efficient than imatinib for the inhibition of activated PDGFRs, but the effective therapy for these tumors may require combined regimens targeting multiple RTKs and/or downstream pathway regulatory effectors.

Disclosure of Potential Conflicts of Interest

No potential conflicts of interest were disclosed.

Acknowledgments

We thank Dr. Pascale Cervera (Hôpital Saint Antoine, Paris, France) for providing tumor tissue biopsy samples for this study.

Grant Support

Fonds voor Wetenschappelijk Onderzoek Vlaanderen grant G.0589.09 (M. Debiec-Rychter) and a Concerted Action Grant (2006/14) from the K.U. Leuven. P. Vandenberghe is a senior clinical investigator of FWO.

The costs of publication of this article were defrayed in part by the payment of page charges. This article must therefore be hereby marked *advertisement* in accordance with 18 U.S.C. Section 1734 solely to indicate this fact.

Received 05/03/2010; revised 06/29/2010; accepted 07/07/2010; published OnlineFirst 08/04/2010.

Published OnlineFirst August 4, 2010; DOI: 10.1158/0008-5472.CAN-10-1543

References

1. Andrae J, Gallini R, Betsholtz C. Role of platelet-derived growth factors in physiology and medicine. Genes Dev 2008;22:1276–312.
2. Heldin CH, Westermark B. Mechanism of action and *in vivo* role of platelet-derived growth factor. Physiol Rev 1999;79:1283–316.
3. Olson LE, Soriano P. Increased PDGFRα activation disrupts connective tissue development and drives systemic fibrosis. Dev Cell 2009;16:303–13.
4. Ostman A, Heldin CH. PDGF receptors as targets in tumor treatment. Adv Cancer Res 2007;97:247–74.
5. Bovee JV, Hogendoorn PC. Molecular pathology of sarcomas: concepts and clinical implications. Virchows Arch 2010;456:193–9.
6. Heinrich MC, Corless CL, Duensing A, et al. PDGFRA activating mutations in gastrointestinal stromal tumors. Science 2003;299:708–10.
7. Sirvent N, Maire G, Pedeutour F. Genetics of dermatofibrosarcoma protuberans family of tumors: from ring chromosomes to tyrosine kinase inhibitor treatment. Genes Chromosomes Cancer 2003;37:1–19.
8. Heinrich MC, Corless CL, Demetri GD, et al. Kinase mutations and imatinib response in patients with metastatic gastrointestinal stromal tumor. J Clin Oncol 2003;21:4342–9.
9. Sjoblom T, Shimizu A, O'Brien KP, et al. Growth inhibition of dermatofibrosarcoma protuberans tumors by the platelet-derived growth factor receptor antagonist STI571 through induction of apoptosis. Cancer Res 2001;61:5778–83.
10. Hermanson M, Funa K, Koopmann J, et al. Association of loss of heterozygosity on chromosome 17p with high platelet-derived growth factor α receptor expression in human malignant gliomas. Cancer Res 1996;56:164–71.
11. Joensuu H, Puputti M, Sihto H, Tynninen O, Nupponen NN. Amplification of genes encoding KIT, PDGFRα and VEGFR2 receptor tyrosine kinases is frequent in glioblastoma multiforme. J Pathol 2005;207:224–31.
12. Smith JS, Wang XY, Qian J, et al. Amplification of the platelet-derived growth factor receptor-A (PDGFRA) gene occurs in oligodendrogliomas with grade IV anaplastic features. J Neuropathol Exp Neurol 2000;59:495–503.
13. Arai H, Ueno T, Tangoku A, et al. Detection of amplified oncogenes by genome DNA microarrays in human primary esophageal squamous cell carcinoma: comparison with conventional comparative genomic hybridization analysis. Cancer Genet Cytogenet 2003;146:16–21.
14. Bode-Lesniewska B, Zhao J, Speel EJ, et al. Gains of 12q13-14 and overexpression of mdm2 are frequent findings in intimal sarcomas of the pulmonary artery. Virchows Arch 2001;438:57–65.
15. Bode-Lesniewska B, Komminoth P. Intimal sarcoma. In: Fletcher CD, Unni KK, Mertens F, editors. World Health Organization classification of tumours. Pathology and genetics of tumours of soft tissue and bone. Lyon: IARC; 2002, p. 223–4.
16. Burke AP, Virmani R. Sarcomas of the great vessels. A clinicopathologic study. Cancer 1993;71:1761–73.
17. Hottenrott G, Mentzel T, Peters A, Schroder A, Katenkamp D. Intravascular ("intimal") epithelioid angiosarcoma: clinicopathological and immunohistochemical analysis of three cases. Virchows Arch 1999;435:473–8.
18. Miracco C, Laurini L, Santopietro R, et al. Intimal-type primary sarcoma of the aorta. Report of a case with evidence of rhabdomyosarcomatous differentiation. Virchows Arch 1999;435:62–6.
19. Nishikawa H, Miyakoshi S, Nishimura S, Seki A, Honda K. A case of aortic intimal sarcoma manifested with acutely occurring hypertension and aortic occlusion. Heart Vessels 1989;5:54–8.
20. Nonomura A, Kurumaya H, Kono N, et al. Primary pulmonary artery sarcoma. Report of two autopsy cases studied by immunohistochemistry and electron microscopy, and review of 110 cases reported in the literature. Acta Pathol Jpn 1988;38:883–96.
21. Thalheimer A, Fein M, Geissinger E, Franke S. Intimal angiosarcoma of the aorta: report of a case and review of the literature. J Vasc Surg 2004;40:548–53.
22. Higgins R, Posner MC, Moosa HH, Staley C, Pataki KI, Mendelow H. Mesenteric infarction secondary to tumor emboli from primary aortic sarcoma. Guidelines for diagnosis and management. Cancer 1991;68:1622–7.
23. Penel N, Taieb S, Ceugnart L, et al. Report of eight recent cases of locally advanced primary pulmonary artery sarcomas: failure of doxorubicin-based chemotherapy. J Thorac Oncol 2008;3:907–11.
24. Tamborini E, Casieri P, Miselli F, et al. Analysis of potential receptor tyrosine kinase targets in intimal and mural sarcomas. J Pathol 2007;212:227–35.
25. Zhao J, Roth J, Bode-Lesniewska B, Pfaltz M, Heitz PU, Komminoth P. Combined comparative genomic hybridization and genomic microarray for detection of gene amplifications in pulmonary artery intimal sarcomas and adrenocortical tumors. Genes Chromosomes Cancer 2002;34:48–57.
26. Knuutila S, Bjorkqvist AM, Autio K, et al. DNA copy number amplifications in human neoplasms: review of comparative genomic hybridization studies. Am J Pathol 1998;152:1107–23.
27. Debiec-Rychter M, Lasota J, Sarlomo-Rikala M, Kordek R, Miettinen M. Chromosomal aberrations in malignant gastrointestinal stromal tumors: correlation with c-KIT gene mutation. Cancer Genet Cytogenet 2001;128:24–30.
28. Tuveson DA, Willis NA, Jacks T, et al. STI571 inactivation of the gastrointestinal stromal tumor c-KIT oncoprotein: biological and clinical implications. Oncogene 2001;20:5054–8.
29. Smeets MF, Mooren EH, Abdel-Wahab AH, Bartelink H, Begg AC. Differential repair of radiation-induced DNA damage in cells of human squamous cell carcinoma and the effect of caffeine and cysteamine on induction and repair of DNA double-strand breaks. Radiat Res 1994;140:153–60.
30. Debiec-Rychter M, Wasag B, Stul M, et al. Gastrointestinal stromal tumours (GISTs) negative for KIT (CD117 antigen) immunoreactivity. J Pathol 2004;202:430–8.
31. Dewaele B, Wasag B, Cools J, et al. Activity of dasatinib, a dual SRC/ABL kinase inhibitor, and IPI-504, a heat shock protein 90 inhibitor, against gastrointestinal stromal tumor-associated PDGFRAD842V mutation. Clin Cancer Res 2008;14:5749–58.
32. Qu Z, Han X, Cui Y, Li C. A PI3 kinase inhibitor found to activate bestrophin 3. J Cardiovasc Pharmacol 2010;55:110–5.
33. Kubo T, Piperdi S, Rosenblum J, et al. Platelet-derived growth factor receptor as a prognostic marker and a therapeutic target for imatinib mesylate therapy in osteosarcoma. Cancer 2008;112:2119–29.
34. Tamborini E, Virdis E, Negri T, et al. Analysis of receptor tyrosine kinases (RTKs) and downstream pathways in chordoma. Neuro-oncol 2010;12:776–89.
35. Guillou L, Aurias A. Soft tissue sarcomas with complex genomic profiles. Virchows Arch 2010;456:201–17.
36. Coindre JM, Pedeutour F, Aurias A. Well-differentiated and dedifferentiated liposarcomas. Virchows Arch 2010;456:167–79.
37. Shangary S, Wang S. Small-molecule inhibitors of the MDM2-53 protein-protein interaction to reactivate p53 function: a novel approach for cancer therapy. Annu Rev Pharmacol Toxicol 2009;49:223–41.
38. Tovar C, Rosinski J, Filipovic Z, et al. Small-molecule MDM2 antagonists reveal aberrant p53 signaling in cancer: implications for therapy. Proc Natl Acad Sci U S A 2006;103:1888–93.
39. Lurje G, Lenz HJ. EGFR signaling and drug discovery. Oncology 2009;77:400–10.
40. Mitsudomi T, Yatabe Y. Epidermal growth factor receptor in relation to tumor development: EGFR gene and cancer. FEBS J 2010;277:301–8.
41. Sato O, Wada T, Kawai A, et al. Expression of epidermal growth factor receptor, ERBB2 and KIT in adult soft tissue sarcomas: a clinicopathologic study of 281 cases. Cancer 2005;103:1881–90.
42. Stewart CF, Leggas M, Schuetz JD, et al. Gefitinib enhances the

Published OnlineFirst August 4, 2010; DOI: 10.1158/0008-5472.CAN-10-1543

antitumor activity and oral bioavailability of irinotecan in mice. Cancer Res 2004;64:7491–9.
43. Messerschmitt PJ, Rettew AN, Brookover RE, Garcia RM, Getty PJ, Greenfield EM. Specific tyrosine kinase inhibitors regulate human osteosarcoma cells *in vitro*. Clin Orthop 2008;466:2168–75.
44. Stommel JM, Kimmelman AC, Ying H, et al. Coactivation of receptor tyrosine kinases affects the response of tumor cells to targeted therapies. Science 2007;318:287–90.
45. Yokoi K, Thaker PH, Yazici S, et al. Dual inhibition of epidermal growth factor receptor and vascular endothelial growth factor receptor phosphorylation by AEE788 reduces growth and metastasis of human colon carcinoma in an orthotopic nude mouse model. Cancer Res 2005;65:3716–25.
46. Zhou Y, Li S, Hu YP, et al. Blockade of EGFR and ErbB2 by the novel dual EGFR and ErbB2 tyrosine kinase inhibitor GW572016 sensitizes human colon carcinoma GEO cells to apoptosis. Cancer Res 2006; 66:404–11.
47. Chen Z, Lee FY, Bhalla KN, Wu J. Potent inhibition of platelet-derived growth factor-induced responses in vascular smooth muscle cells by BMS-354825 (dasatinib). Mol Pharmacol 2006;69: 1527–33.
48. Li J, Rix U, Fang B, et al. A chemical and phosphoproteomic characterization of dasatinib action in lung cancer. Nat Chem Biol 2010;6: 291–9.
49. Sato K, Nagao T, Iwasaki T, Nishihira Y, Fukami Y. Src-dependent phosphorylation of the EGF receptor Tyr-845 mediates Stat-p21waf1 pathway in A431 cells. Genes Cells 2003;8:995–1003.
50. Yoshida T, Okamoto I, Okamoto W, et al. Effects of Src inhibitors on cell growth and epidermal growth factor receptor and MET signaling in gefitinib-resistant non-small cell lung cancer cells with acquired MET amplification. Cancer Sci 2010;101:167–72.
51. Paterson AL, Pole JC, Blood KA, et al. Co-amplification of 8p12 and 11q13 in breast cancers is not the result of a single genomic event. Genes Chromosomes Cancer 2007;46:427–39.

Published OnlineFirst August 4, 2010; DOI: 10.1158/0008-5472.CAN-10-1543

AACR American Association for Cancer Research

Cancer Research

The Journal of Cancer Research (1916–1930) | The American Journal of Cancer (1931–1940)

Coactivated Platelet-Derived Growth Factor Receptor α and Epidermal Growth Factor Receptor Are Potential Therapeutic Targets in Intimal Sarcoma

Barbara Dewaele, Giuseppe Floris, Julio Finalet-Ferreiro, et al.

Cancer Res 2010;70:7304-7314. Published OnlineFirst August 4, 2010.